

THE UNIVERSITY of EDINBURGH

Edinburgh Research Explorer

Disease-specific oligodendrocyte lineage cells arise in multiple sclerosis

Citation for published version:

Mendanha Falcão, A, van Bruggen, D, Marques, S, Meijer, M, Jaekel, S, Agirre, E, Samudyata, Floriddia, EM, Vanichkina, DP, ffrench-Constant, C, Williams, A, Ortlieb Guerreiro-Cacais, A & Castelo-Branco, G 2018, 'Disease-specific oligodendrocyte lineage cells arise in multiple sclerosis', *Nature Medicine*, vol. 24, no. 12, pp. 1837–1844. https://doi.org/10.1038/s41591-018-0236-y

Digital Object Identifier (DOI):

10.1038/s41591-018-0236-y

Link:

Link to publication record in Edinburgh Research Explorer

Document Version: Peer reviewed version

Published In: Nature Medicine

General rights

Copyright for the publications made accessible via the Edinburgh Research Explorer is retained by the author(s) and / or other copyright owners and it is a condition of accessing these publications that users recognise and abide by the legal requirements associated with these rights.

Take down policy The University of Edinburgh has made every reasonable effort to ensure that Edinburgh Research Explorer content complies with UK legislation. If you believe that the public display of this file breaches copyright please contact openaccess@ed.ac.uk providing details, and we will remove access to the work immediately and investigate your claim.



1 2	Disease-specific oligodendrocyte lineage cells arise in multiple sclerosis
3 4	Ana Mendanha Falcão ^{1*} , David van Bruggen ^{1*} , Sueli Marques ¹ , Mandy Meijer ¹ ,
5	Sarah Jäkel ² , Eneritz Agirre ¹ , Samudyata ¹ , Elisa M. Floriddia ¹ , Darya P.
6	Vanichkina ^{3,4} , Charles ffrench-Constant ² , Anna Williams ² , André Ortlieb Guerreiro-
7	Cacais ⁵ , Gonçalo Castelo-Branco ^{1,6}
8	¹ Laboratory of Molecular Neurobiology, Department Medical Biochemistry and Biophysics,
9	Karolinska Institutet, Biomedicum, 17177 Stockholm, Sweden
10	² MRC Centre for Regenerative Medicine, Edinburgh bioQuarter, University of Edinburgh, Edinburgh,
11	EH16 4UU, United Kingdom
12	³ Gene and Stem Cell Therapy Program, Centenary Institute, University of Sydney, Camperdown,
13	NSW 2050, Australia
14	⁴ Institute for Molecular Bioscience, University of Queensland, St Lucia, QLD 4067, Australia
15	⁵ Department of Clinical Neuroscience (CNS), Karolinska Institutet, CMM 17176 Stockholm, Sweden
16	⁶ Ming Wai Lau Centre for Reparative Medicine, Stockholm node, Karolinska Institutet, 171 77
17	Stockholm, Sweden
18	
19	
20	* These authors contributed equally
21	
22	Correspondence: ana.mendanha.falcao@ki.se and goncalo.castelo-branco@ki.se
23	
24	One Sentence Summary: Single-cell RNA-seq of a mouse model of multiple
25	sclerosis uncovers new oligodendrocyte populations, putative disease markers and
26	suggests new mechanisms underlying the pathogenesis of disease.
27	
28	
29	

30 Introductory paragraph (202 words)

31 Multiple Sclerosis (MS) is characterised by an immune system attack targeting 32 myelin, which is produced by oligodendrocytes (OLs). We performed single-cell 33 transcriptomic analysis of OL lineage cells from the spinal cord of mice induced 34 with experimental autoimmune encephalomyelitis (EAE), which mimics several 35 aspects of MS. We found unique OLs and OL precursor cells (OPCs) in EAE 36 and uncovered several genes specifically alternatively spliced in these cells. 37 Surprisingly, EAE-specific OL-lineage populations expressed genes involved in 38 antigen processing and presentation via major histocompatibility complex class I 39 and II (MHC-I and -II), and in immunoprotection, suggesting alternative 40 functions of these cells in a disease context. Importantly, we found that disease-41 specific oligodendroglia are also present in human MS brains and that a 42 substantial number of genes known to be susceptibility genes for MS, so far 43 mainly associated with immune cells, are expressed in the OL lineage cells. 44 Finally, we demonstrate that OPCs can phagocytose and that MHC-II expressing 45 OPCs can activate memory and effector CD4+ T cells. Our results suggest that 46 OLs and OPCs are not passive targets but instead active immunomodulators in 47 MS. The disease-specific OL lineage cells, for which we identify several 48 biomarkers, may represent novel direct targets for immunomodulatory 49 therapeutic approaches in MS.

50

51 (main text: 3055 words)

52 The adaptive immune system is currently thought to be the most likely aetiological 53 component for MS, although microglia have been suggested to also have a role^{1,2}. We 54 have shown that OLs, whose myelin is thought to be a passive target of the immune system in MS, are heterogeneous in mouse^{3,4}. To investigate whether specific OL 55 56 populations are targeted in MS, we isolated single cells from the spinal cord of control 57 (treated with Complete Freund's Adjuvant, CFA) or EAE mice (Fig. 1a). Cells from 58 EAE mice were collected at the peak of the disease (score=3, indicating total hindlimb paralysis, Fig. 1b) and we performed Smart-seq2⁵ single cell RNA-seq (Fig. 59 1a). OL-lineage cells were isolated by fluorescence activated cell sorting (FACS) 60 GFP+ cells from EAE-induced Pdgfra-H2B-GFP transgenic mice⁶ (enriching for 61 62 OPCs and "young" OLs, that had differentiated recently), and Pdgfra-Cre-LoxP-

GFP⁷, (containing mainly "old" OL-lineage cells labelled with GFP since early
development, but also "young" OLs and OPCs; Fig. 1a and Supplementary Fig. 1a).

65

66 EAE mice spinal cord cells segregated from CFA control mice, with a subset of 67 clusters uniquely found in EAE (Fig. 1c, Supplementary Fig. 1b,e). Clustering 68 analysis (GeneFocus pipeline, see Methods and Supplementary Fig. 2) revealed 69 thirteen OL lineage clusters, including four clusters of OPCs, one differentiation-70 committed oligodendrocyte precursor (COP), one newly formed OL (NFOL) and 71 eight mature OL (MOLs; Fig. 1d and Supplementary Fig. 1b). We also identified vascular and leptomeningeal cells (VLMCs)^{3,4}, consistent with the labelling of this 72 population with *Pdgfra*, and microglia-like cells (which, while they could also include 73 74 macrophages, we refer to as microglia; Fig. 1c and Supplementary Fig. 1b), which 75 could reflect transient Pdgfra expression in these cells, or phagocytosis of myelin-76 associated GFP.

77

EAE-enriched OPC populations comprised OPCcyc (cycling), OPC2 and OPC3; 78 79 distinct from the OPC1 population found in healthy mice (Supplementary Fig. 1e) that 80 shares transcriptional profile similar to previously identified postnatal and adult mouse OPCs^{3,4} (Fig. 1e and Supplementary Fig. 3d-f). Dimensionality reduction using 81 82 non-negative matrix factorization (NNMF) yielded a rank of 8 components (see 83 Methods). Removal of components 7 and 8 that correlated to S and G2 phase cell-84 cycle genes revealed that OPCcyc can be further deconvoluted, suggesting that the 85 OPCcyc population describes a mixture of cell state transitions from OPC1, OPC2 86 and OPC3 (Supplementary Fig. 3). Comparison of OPC populations showed specific 87 expression of genes such as *Rph3a*, *Adora2b* in OPC1, *Phyhd1*, *Sult1a1* in OPC2 and 88 Slc14a1 in OPC3 (Fig. 1e and Supplementary Table 1). OPC2 and OPC3 clusters 89 displayed unique expression of *Fcgr2b*, *Mylk*, *Lgals1* (Fig. 1e, g, Supplementary Fig. 4a and Supplementary Table 1), when compared to OPC1, and increased levels of 90 *Myrf* (Fig. 1e), a transcription factor necessary for myelination⁸, and decreased levels 91 of *Hes1* and *Hes5* (Supplementary Fig. 4a), that keep OPCs in a progenitor state⁹. The 92 93 COPs and NFOLs expressing *Col20a1* (Fig. 1g) and *Syt4* (Supplementary Fig. 4a) 94 were mostly from EAE mice. Thus, OPCs undergo proliferation and differentiation in EAE^{10,11}, but also transition to previously unidentified transcriptional states. 95

96

MOLs presented several markers identified in Margues et al.⁴, and could be 97 98 subcategorized accordingly (Fig. 1d, f and Supplementary Fig. 1c). EAE-associated 99 MOL lineage populations expressed unique genes, absent or very low expressed in 100 healthy controls. Klk8, Itga8, Tlr3, Trim34a were enriched in MOL1/2-EAE; Plin4, 101 Sult1a1 and Zfand4 in MOL5/6-EAE-a; and S100a10, RNAse4 and Tnfrsf1a, a MS susceptibility gene,¹² in MOL5/6-EAE-b (Fig. 1f. g. Supplementary Fig. 4a and 102 103 Supplementary Table 1). We found disease-specific markers in OL lineage cells such 104 as Igtp, Nlrc5, and Serpina3n (Fig. 2b and Supplementary Fig. 4a). Ill2rb1 was 105 present in all MOL populations found in EAE mice (Fig. 1g). All OL lineage clusters 106 comprised cells from both transgenic mouse lines, with the exception of MOL5/6-107 EAE-a, from Pdgfra-H2B-GFP mice, which might thus be composed of "young" OLs 108 (Supplementary Fig. 1e).

109

110 To identify gene-transcription trends, we decomposed the dataset into components 111 using NNMF (Supplementary Fig. 4b) and found 19 robust gene modules, including 112 two that were uniquely associated with EAE: module 1, present in a subset of EAE 113 cells comprising genes related to interferon response pathways and MHC-I and -II 114 genes, and module 13 restricted to the MOL5/6-EAE-a population, which contained 115 genes such as *Plin4*, *Hif3a*, and *Fam107a* (Supplementary Fig. 4b). Similar results 116 were obtained when performing GO/Reactome analysis (Supplementary Fig. 4c and 117 5a, and Supplementary Table 3). We also uncovered 360 genes that were alternatively 118 spliced in EAE OL-lineage cells, with either exon exclusion or inclusion 119 (Supplementary Table 2). Gene Ontology (GO)/reactome analysis showed that genes 120 with alternatively spliced exons in EAE OPCs were related to regulation of 121 transcriptional elongation from RNA Pol II (exon exclusion), membrane trafficking 122 (exon inclusion), and RNA-splicing components (exon exclusion; Supplementary Fig. 123 5b and Supplementary Table 3). We also found evidence of alternative splicing in 124 EAE in several genes involved in myelination and MS, including the myelin genes Mbp (as previously reported¹³), Mobp, Pdgfa and the Ifih1 gene, in which MS-125 associated polymorphisms have been found¹⁴ (Fig. 1.h, i Supplementary Fig. 5c and 126 127 Supplementary Table 2).

128

We performed RNAscope *in situ* hybridization (ISH) and immunohistochemistry(IHC) in EAE spinal cords, against several markers of the identified clusters, such as

131 Klk8, which specifically marks MOL1/2-EAE (Fig. 1g) and Hopx, which marks $MOL2^4$. While control spinal cords exhibited sparse *Klk8* expression we observed a 132 133 strong induction of *Klk8* in a subset of $Hopx^+/Sox10^+$ MOL2 in EAE mice (Fig. 2a). 134 We also confirmed the presence of PLIN4 protein (enriched in MOL5/6 EAE-a) by 135 performing IHC on spinal cords and found elevated GFP/PLIN4 double positive cells 136 (from the Pdgfra-H2B-GFP mouse) and Sox10/PLIN4 (Supplementary Fig. 6a) in 137 EAE mice. Thus, Klk8 and Plin4 are new markers of subpopulations of EAE-138 responsive MOLs.

139

140 All oligodendroglia in EAE displayed elevated Serpina3n expression (Fig. 2b), 141 encoding a serine protease inhibitor that has been shown to reduce EAE severity and 142 induce neuroprotection¹⁵. We confirmed the increase in *Serpina3n* in EAE by 143 RNAscope ISH, especially notable within $Sox10^+$ cells (Fig. 2c). The expression of 144 this molecule reached such high levels in EAE, that we could no longer detect single 145 dots. Interestingly, we found expression of additional genes of the Serpina3 family, 146 including Serpina3h, Serpina3c, Serpina3i, Serpina3f and Serpina3g specific to 147 MOL1/2-EAE (Fig. 2b), which could suggest that this population might be protected 148 against direct damage by T- or NK-cells. This population also expresses the gene 149 Serping1 (Fig. 2b) encoding for an inhibitor of complement activation, another 150 possible mechanism of immunoprotection.

151

152 MHC-I genes such as H2-K1, H2-D1, H2-T23, B2m, and genes necessary for antigen 153 processing and binding to MHC-I molecules, such as *Psmb9*, *Tap1* and *Tap2* were 154 significantly increased upon EAE induction in OL lineage cells (Fig. 2d and 155 Supplementary Table 1). Thus, EAE OLs might be direct targets of cytotoxic T cells, 156 which is consistent with their expression of myelin epitopes. Surprisingly, however, 157 we found that OPCs also exhibited a robust increase in the expression of these 158 molecules (Fig. 2d), suggesting that OPCs might also be targeted during the disease, 159 despite not expressing myelin proteins. To validate the expression of MHC-I 160 molecules in oligodendroglia cells, we have performed RNAscope ISH and observed 161 an upregulation of B2m molecules in $Sox10^+$ cells in EAE spinal cords as well as the presence of *Psmb9* molecules in $Sox10^+$ cells in EAE that were absent in $Sox10^+$ cells 162 163 in control spinal cords (Fig. 2e).

164

165 MHC-II genes are thought to be restricted to microglia/macrophages in MS, and not 166 present in OLs in active lesions¹⁶. Strikingly, we found the expression of all key genes 167 required for a MHC-II mediated response, including H2-aa, H2-ab1, H2-eb1, Cd74 168 and Ctss, in specific subsets of OPCs and OLs (Fig. 3a). To confirm the presence of 169 these RNA transcripts in OL lineage cells, we performed RNAscope ISH in the EAE 170 and control spinal cords using probes targeting Cd74 and H2-Eb1 (for MHC-II), in 171 combination with *Aif1* (for microglia), *Sox10* (for OL lineage cells), *Klk6* (for MOL2) 172 and *Ptprz1* (for OPC) (Fig. 3b-d, Supplementary Fig. 6b, and Supplementary Videos 173 V1-V6). While we observed microglia processes enwrapping OLs (Supplementary 174 video V7), a small proportion of OLs/OPCs could be confidently assigned with 175 double positive Cd74/Sox10 and few or no molecules for Aif1 (Fig. 3d and 176 Supplementary Videos V1-V6). We also combined RNAscope ISH with 177 immunohistochemistry and found triple positive OPCs for GFP (from EAE Pdgfra-178 H2B-GFP spinal cord), *Ptprz1* and *Cd74* (Fig. 3c and Supplementary video V2). We 179 also performed IHC for MHC-II and the OL markers OLIG2 and SOX10, and 180 identified double positive cells for OLIG2/MHC-II and SOX10/MHC-II 181 oligodendroglia in the spinal cord of EAE mice (Fig. 3e and Supplementary Fig. 6c). 182 We estimated that in the lesion areas of the white matter SOX10/MHC-II double 183 oligodendroglia constitute about 3.4% (+/-1.76 SD) of the SOX10⁺ cells. We 184 performed IBA-1 staining to distinguish between SOX10/MHC-II oligodendroglia 185 and MHC-II expressing macrophages/microglia and we could distinguish the two cell 186 types. Nevertheless, IBA-1 could still be observed in SOX10/MHC-II oligodendroglia 187 although with a lower expression, which could be due to induction of some Aif1 188 molecules (corresponds to IBA-1 protein) in oligodendroglia in EAE, by for instance interferon-gamma $(IFN\gamma)^{17}$. Control CFA-treated spinal cord OPCs/OLs did not 189 190 express MHC-II molecules neither at the RNA (RNAscope ISH) nor protein level 191 (IHC; Fig. 3b and data not shown).

192

We found several interferon responsive genes in MHC-II expressing OL/OPC populations, such as *Ifih1*, *Iigp1*, *Trim34*, *Irf7*, *Irgm1*, *Irgm2*, *Igtp* and *Zbp1* (Supplementary Fig. 7a). It has been shown that IFN γ can trigger endoplasmic reticulum stress in OLs¹⁸. Indeed, we found many genes involved in protein processing in endoplasmic reticulum differentially expressed in EAE (Supplementary Fig. 7b). Transcription factors such as *Nlrc5*, a transactivator of the MHC-I¹⁹, was expressed upon disease in all OL lineage cells, and *Ciita*, induced by the IFNγ
pathway and activator of MHC-II genes, was expressed in a subset of these cells
(Supplementary Fig. 4a). Thus, OL/OPC populations in the spinal cord appear to have
the capacity to activate MHC genes upon EAE induction.

203

204 To determine if these populations also occur in human MS, we performed IHC for 205 MHC-II and the OL markers OLIG2 and OLIG1 in postmortem brain tissue from two 206 MS patients. As in mouse model EAE, we observed cells in which immune cell-207 derived MHC-II processes appear to touch/enwrap OLIG2⁺ nuclei (Supplementary 208 Fig. 6d arrowheads and Supplementary video V8) but also OLIG2 and OLIG1 cells 209 positive for MHC-II without any immune cell in their neighborhood (Fig. 3f and 210 Supplementary Fig. 6d arrows, and Supplementary video V9), indicating that indeed 211 human OLs can express adaptive immunity proteins in the context of MS.

212

213 Several MS susceptibility variants including MHC and autosomal non-MHC locus 214 and the associated putative susceptibility genes were recently described¹. Comparison 215 of these loci/genes with RNA-seq from bulk brain led to the inference that peripheral 216 immune system cells and brain resident microglia were the most likely cell types to 217 contribute to MS susceptibility¹. To examine if MS susceptibility genes were also 218 expressed in OL lineage cells in EAE, we analyzed the expression of the mouse 219 homologs for genes associated with the 200 non-MHC, 32 MHC loci, and 19 X-220 chromosomal loci in our single-cell transcriptomics dataset (Fig. 3g and 221 Supplementary Fig. 6e and Supplementary Table S4). Interestingly, the MHC-II gene 222 H2.Aa (human HLA-DQA1) was enriched not only in microglia, but also in EAE-223 derived OPCs and MOLs (Fig. 3g). Strikingly, several OL lineage cells expressed 224 non-MHC locus associated susceptibility genes (Fig. 3g and Supplementary Table 225 S4). This was particular strong for OPCs (importantly both from control and EAE 226 mice) and MOL1/2-EAE populations (Fig. 3g). OPCs expressed 61% of these genes, 227 which was in the same range as microglia (67%). Moreover, while we found many 228 genes are equally expressed in all the populations, there were also genes enriched in 229 OL lineage cells (such as Bcas1 and Sox8), MOLs (Prr51), OPCs (such as Kcnh8, 230 *Pkia*, *Pitpnm2*) and microglia (such as *Plek*; Supplementary Table S4). Interestingly, 231 a subset of genes starts to be expressed and is upregulated in response to the disease 232 in MOL populations, in particular MOL1/2-EAE.

234 To investigate the mechanism triggering MHC-II expression in OL lineage cells and 235 the functional implications in the development of the disease, we performed co-236 cultures of GFP⁺ OPCs (from Sox10Cre-GFP mice brains) and CD45⁺ immune cells 237 isolated from the spinal cord of EAE mice (Fig. 4a). After 72 hours of co-culture, 238 4.4% (+/-2.42 SD) of the total GFP+ OPCs in culture were positive for MHC-II (Fig. 4b). We also performed co-cultures of OPCs with CD45⁺ immune cells from CFA 239 240 mice (most likely comprising of microglia/macrophages and few invading leukocytes 241 from the periphery) and did not find any GFP/MHC-II double positive OPCs in these 242 conditions (Supplementary Fig. 8a). This indicates that factors secreted by EAE-243 specific immune cells are inducing MHC-II expression in OPCs. Indeed, while MHC-II expression has been reported to be excluded from OLs in MS¹⁶, expression of these 244 245 molecules in rat OPCs and OLs has been observed, upon dexamethasone and IFNy 246 treatment²⁰. As CD4 lymphocytes such as Th1 and memory T cells are interferon-247 producing cells, we hypothesized that the observed effect in the co-cultures was 248 mediated by lymphocyte derived IFN γ . As such, we treated OPCs with IFN γ (100 249 ng/ml, dexamethasone (1µM) and the combination of both for 3 days (Fig. 4c). We 250 observed the induction of expression of MHC-II molecules, in OPCs and OLs, only in 251 IFN γ treated cells, alone or in combination with dexamethasone, both at the RNA 252 level (RNAscope ISH) and protein level (shown by ICC; Fig. 4d and Supplementary 253 Fig. 8b-c). We did not find any positive cell for Aif1 RNA molecules in our MACS 254 OPC primary cultures, nor IBA-1 positive cells, indicating that microglia were absent 255 and excluding the possibility that MHC-II RNA and protein were derived from 256 microglia processes. qPCR analysis further confirmed these results. While genes such 257 as *Plin4*, were not affected by IFNy treatment but only to dexamethasone, we 258 observed a dramatic induction of interferon responsive genes (Ifit2, Ifih1) MHC-II 259 genes (Cd74) and MHC-II and I transactivators (Ciita, Nlrc5) (Fig. 4e). Thus, our 260 results indicate that MHC-II genes induction in EAE OL lineage cells is possibly 261 mediated by IFN γ .

262

To uncover the role of immunocompetent OPCs in the disease, we first investigated if OPCs were capable of phagocytosis, by adding $1\mu m$ diameter fluorescent microspheres to OPC cultures for 24h. OPCs could indeed uptake several

266 microspheres, with at least 48% of them exhibiting this capability (Fig. 4f). Moreover, 267 treatment with the phagocytosis inhibitor cytochalasin D at two different 268 concentrations for 24 hours, lead to a remarkable reduction in microsphere uptake 269 (Fig. 4f, g). IFNy treatment did not alter OPC phagocytic capacity (Fig. 4g). To 270 further investigate whether OPCs can phagocytise myelin, we incubated OPCs for 6 271 hours with pHrodo-labeled myelin (a pH-sensitive fluorogenic dye that fluoresce red in phagosomes²¹) and found that OPCs were able to uptake myelin as observed by the 272 273 red fluorescence staining of live OPCs (Fig. 4f). Altogether, these data demonstrate 274 that OPCs exhibit phagocytic activity and strongly suggests that OPCs are capable of 275 taking up myelin debris in a disease context.

276

277 Next, we addressed the impact of MHC-II expressing OPCs on the survival, 278 proliferation and cytokine production of CD4⁺ T cells derived from 2D2 mice, where T cells express the T cell receptor for the MOG35-55 $peptide^{22}$. OPCs (controls or 279 280 pre-treated with IFNy and/or MOG35-55 peptide) were co-cultured for 72 hours with 281 either naïve, memory or effector T cells (naïve cells that had been pre-activated in 282 *vitro* in the presence of IL-12, acquiring a Th1 phenotype). T cells were subsequently 283 assessed by flow cytometry for survival (cell dead exclusion), proliferation ($Ki67^+$), 284 as well as for expression of IFNy and TNF (Fig. 4h). Co-culturing with non-285 stimulated OPCs lead to an increase in numbers of surviving naïve, activated and 286 memory T cells. Survival was further enhanced in memory T cells when OPCs were 287 pre-treated in IFNy and MOG peptide suggesting an MHC-II mediated effect (Fig. 4i, 288 Supplementary Figs. 8e and 9). Regarding proliferation, naïve CD4⁺ T cells seemed 289 unaffected by OPC co-culture (Fig. 4j and Supplementary Figs. 8e and 9), as 290 expected, since these cells have a high threshold of activation provided in secondary lymphoid tissue. In contrast, we found a higher number of Ki67⁺ memory CD4⁺ T 291 292 cells when co-cultured with OPCs in the presence of MOG peptide. Similar effects 293 were observed for Th1 CD4⁺ T cells which proliferated more in the presence of OPCs 294 and MOG peptide. These results also suggest that the proliferation effect is via OPC-295 MOG peptide presentation to memory and Th1 T cells. Of notice, the presence of 296 MOG peptide, not necessarily together with IFN γ , was enough to induce proliferation. 297 This indicates that production of IFNy by memory and Th1 cells may provide a 298 positive regulatory feedback loop. We thus investigated if the increase in 299 survival/proliferation was accompanied by cytokine production. Indeed, memory

300 $CD4^+$ T cells displayed more cells producing both TNF and IFN γ when co-cultured 301 with OPCs in the presence of MOG peptide (Supplementary Fig. 8d). In contrast, the 302 presence of OPCs per se triggered an increase in the number of Th1 CD4⁺ T cells 303 producing IFN γ and TNF (Supplementary Fig. 8d).

304

305 OLs are widely seen as a passive target of a dysregulated immune system, but there is 306 a growing body of evidence of immunomodulatory factors expressed in OLs such as cytokines/chemokines and their receptors²³⁻²⁷. Our results indicate that both OPCs and 307 308 MOLs undergo a transcriptional overhaul during chronic inflammatory 309 demyelination. The selective expression of immunoprotective, innate and adaptive 310 immunity genes in OPCs and OLs in EAE suggests potential mechanisms of 311 protection and an immune function in the context of disease. Since several of these 312 genes are susceptibility genes for MS, the OL lineage might have a more central role 313 in the origin and progression of MS than previously thought.

314

315 OL cell death has been recently shown to lead to an adaptive auto-immune response²⁸, 316 which could imply an initial dysregulation in cells of the OL lineage as a triggering 317 event in MS and support the "inside-out" hypothesis for the aetiology of the disease²⁸. 318 Whether the new identified OL lineage cell states play a role on the aetiology of MS, 319 by acting as antigen presenting cells and triggering immunologic attack or reinforcing 320 the disease-initiating event from the periphery, or both, will require further 321 investigation. In either case, our results indicate that OL lineage cells may not simply 322 be passive targets of the immune system in MS, but rather central players which may 323 be targeted in therapeutic approaches for MS.

Accession codes and data availability: A web resource for browsing differential gene expression data for the single cell data can be accessed at <u>https://ki.se/en/mbb/oligointernode</u>. Raw data is deposited in GEO, accession number GSE113973. Code used for single cell RNA-Seq analysis is available at <u>https://github.com/Castelo-Branco-lab/GeneFocus</u>.

329

330 Acknowledgements

331 We would like to thank Alessandra Nanni, Ahmad Moshref, Johnny Söderlund for laboratory 332 management and support. We thank Single Cell Genomics Facility, WABI Long Term 333 Bioinformatic Support (Leif Wigge) at SciLifeLab, the FACS facilities at CMB (Belinda 334 Panagel), Science for Life Laboratory, the National Genomics Infrastructure (NGI) and 335 Uppmax for providing assistance in massive parallel sequencing and computational 336 infrastructure. We want to acknowledge Antonio Gigliotti Rothfuchs for advice and reagents, 337 Marek Bartosovic for assistance, Rasmus Berglund and Marie N'diaye for providing the tools 338 to perform the phagocytosis experiments. The bioinformatics computations were performed 339 on resources provided by the Swedish National Infrastructure for Computing (SNIC) at 340 UPPMAX, Uppsala University. Post mortem MS tissue used for IHC was provided via a UK 341 prospective donor scheme with full ethical approval from the UK Multiple Sclerosis Tissue 342 Bank (MREC/02/02/39). D.P.V. would like to acknowledge the University of Sydney HPC 343 service at The University of Sydney for providing HPC resources that have contributed to the 344 research reported in this paper. This work was supported in part by a University of Sydney 345 HPC Grand Challenge Award. D.P.V. was supported in part by a Boehringer Ingelheim 346 Travel Grant. C.f.-C. is funded by a Wellcome Trust Investigator award. AW is funded by 347 UK Multiple Sclerosis Society. SJ is funded by European Union, Horizon 2020, Marie-348 Skłodowska Curie Actions, grant number EC reference number 789492. A.M.F. by the 349 European Committee for Treatment and Research of Multiple Sclerosis (ECTRIMS). EA is 350 funded by European Union, Horizon 2020, Marie-Skłodowska Curie Actions, grant SOLO, 351 number 794689. Work in G.C.-B.'s research group was supported by Swedish Research 352 Council (grant 2015-03558), European Union (Horizon 2020 Research and Innovation 353 Programme/ European Research Council Consolidator Grant EPIScOPE, grant agreement 354 number 681893), Swedish Brain Foundation (FO2017-0075), Ming Wai Lau Centre for 355 Reparative Medicine, Petrus och Augusta Hedlunds Foundation ((grants M-2014-0041 and 356 M-2016-0428) and Karolinska Institutet.

357

358 Author Contributions: A.M.F., D.V.B and G.C.-B. conceived the project, designed 359 the study and interpreted results. A.M.F., S.M. and A.O.G-C. performed EAE model 360 and A.M.F and S.M. collected single cells to generate single-cell sequencing data. 361 D.V.B and E.A. performed computational analyses. A.M.F and M.M. designed, 362 performed and analyzed most in vitro OPC experiments and S. performed the 363 phagocytosis experiments together with A.M.F. A.O.G-C. and A.M.F. designed, 364 performed and analyzed all experiments involving co-cultures with immune cells. 365 S.J., A.W. and C.f.-C. provided the human postmortem MS brain tissue and 366 performed the human IHC analysis. D.P.V. provided support for computational

- 367 analysis. E.M.F. provided RNAscope ISH expertise and performed all videos. A.M.F,
- 368 D.V.B and G.C.-B. wrote the manuscript with feedback from all authors.
- 369

370 Competing interests:

- 371 The G.C-B research group has received funding from F. Hoffmann La Roche, Ltd.
- 372 for another research project in the area.
- 373
- 374 Additional information: Reprints and permissions information is available at
- 375 www.nature.com/reprints. Readers are welcome to comment on the online version of
- the paper. Correspondence and requests for materials should be addressed to G.C.-B.
- 377 (goncalo.castelo-branco@ki.se).
- 378
- 379

380 References

- 381
- 382 Patsopoulos, N. et al. The Multiple Sclerosis Genomic Map: Role of peripheral 1 383 immune cells and resident microglia in susceptibility. *bioRxiv*, doi:10.1101/143933 (2017). 384 Skene, N. G. & Grant, S. G. Identification of Vulnerable Cell Types in Major Brain 2 385 Disorders Using Single Cell Transcriptomes and Expression Weighted Cell Type Enrichment. 386 Front Neurosci 10, 16, doi:10.3389/fnins.2016.00016 (2016). 387 Marques, S. et al. Transcriptional Convergence of Oligodendrocyte Lineage 3 388 Progenitors during Development. Dev Cell 46, 504-517 e507, 389 doi:10.1016/j.devcel.2018.07.005 (2018). 390 4 Marques, S. et al. Oligodendrocyte heterogeneity in the mouse juvenile and adult 391 central nervous system. Science 352, 1326-1329 (2016).
- 392 5 Picelli, S. *et al.* Smart-seq2 for sensitive full-length transcriptome profiling in single
 393 cells. *Nat Methods* 10, 1096-1098, doi:10.1038/nmeth.2639 (2013).
- Klinghoffer, R. A., Hamilton, T. G., Hoch, R. & Soriano, P. An allelic series at the
 PDGFalphaR locus indicates unequal contributions of distinct signaling pathways during
 development. *Dev Cell* 2, 103-113 (2002).
- Kang, S. H., Fukaya, M., Yang, J. K., Rothstein, J. D. & Bergles, D. E. NG2+ CNS
 glial progenitors remain committed to the oligodendrocyte lineage in postnatal life and
- 399 following neurodegeneration. *Neuron* **68**, 668-681, doi:10.1016/j.neuron.2010.09.009 (2010).
- 400 8 Emery, B. *et al.* Myelin gene regulatory factor is a critical transcriptional regulator 401 required for CNS myelination. *Cell* **138**, 172-185, doi:10.1016/j.cell.2009.04.031 (2009).
- required for CNS myelination. *Cell* 138, 172-185, doi:10.1016/j.cell.2009.04.031 (2009).
 Ogata, T. *et al.* Hes1 functions downstream of growth factors to maintain
- 403 oligodendrocyte lineage cells in the early progenitor stage. *Neuroscience* 176, 132-141,
 404 doi:10.1016/j.neuroscience.2010.12.015 (2011).
- Tripathi, R. B., Rivers, L. E., Young, K. M., Jamen, F. & Richardson, W. D. NG2
 glia generate new oligodendrocytes but few astrocytes in a murine experimental autoimmune
 encephalomyelitis model of demyelinating disease. *J Neurosci* **30**, 16383-16390,
- 408 doi:10.1523/JNEUROSCI.3411-10.2010 (2010).
- 409 11 Zawadzka, M. *et al.* CNS-resident glial progenitor/stem cells produce Schwann cells
 410 as well as oligodendrocytes during repair of CNS demyelination. *Cell Stem Cell* 6, 578-590,
 411 doi:10.1016/j.stem.2010.04.002 (2010).
- 412 12 Gregory, A. P. *et al.* TNF receptor 1 genetic risk mirrors outcome of anti-TNF
- 413 therapy in multiple sclerosis. *Nature* **488**, 508-511, doi:10.1038/nature11307 (2012).

414 13 Capello, E., Voskuhl, R. R., McFarland, H. F. & Raine, C. S. Multiple sclerosis: re-415 expression of a developmental gene in chronic lesions correlates with remyelination. Annals 416 of neurology 41, 797-805, doi:10.1002/ana.410410616 (1997). 417 14 Enevold, C. et al. Multiple sclerosis and polymorphisms of innate pattern recognition 418 receptors TLR1-10, NOD1-2, DDX58, and IFIH1. Journal of neuroimmunology 212, 125-419 131, doi:10.1016/j.jneuroim.2009.04.008 (2009). 420 15 Haile, Y. et al. Granzyme B-inhibitor serpina3n induces neuroprotection in vitro and 421 in vivo. Journal of neuroinflammation 12, 157, doi:10.1186/s12974-015-0376-7 (2015). 422 Lee, S. C. & Raine, C. S. Multiple sclerosis: oligodendrocytes in active lesions do not 16 423 express class II major histocompatibility complex molecules. Journal of neuroimmunology 424 25, 261-266 (1989). 425 17 Sibinga, N. E., Feinberg, M. W., Yang, H., Werner, F. & Jain, M. K. Macrophage-426 restricted and interferon gamma-inducible expression of the allograft inflammatory factor-1 427 gene requires Pu.1. J Biol Chem 277, 16202-16210, doi:10.1074/jbc.M200935200 (2002). 428 18 Lin, W., Harding, H. P., Ron, D. & Popko, B. Endoplasmic reticulum stress 429 modulates the response of myelinating oligodendrocytes to the immune cytokine interferon-430 gamma. J Cell Biol 169, 603-612, doi:10.1083/jcb.200502086 (2005). 431 19 Kobayashi, K. S. & van den Elsen, P. J. NLRC5: a key regulator of MHC class I-432 dependent immune responses. Nature reviews. Immunology 12, 813-820, doi:10.1038/nri3339 433 (2012).434 20 Bergsteindottir, K., Brennan, A., Jessen, K. R. & Mirsky, R. In the presence of 435 dexamethasone, gamma interferon induces rat oligodendrocytes to express major 436 histocompatibility complex class II molecules. Proceedings of the National Academy of 437 Sciences of the United States of America 89, 9054-9058 (1992). 438 21 Brosius Lutz, A. et al. Schwann cells use TAM receptor-mediated phagocytosis in 439 addition to autophagy to clear myelin in a mouse model of nerve injury. Proc Natl Acad Sci U 440 *S A* **114**, E8072-E8080, doi:10.1073/pnas.1710566114 (2017). 441 Bettelli, E. et al. Myelin oligodendrocyte glycoprotein-specific T cell receptor 22 442 transgenic mice develop spontaneous autoimmune optic neuritis. J Exp Med 197, 1073-1081, 443 doi:10.1084/jem.20021603 (2003). 444 23 Zeis, T., Enz, L. & Schaeren-Wiemers, N. The immunomodulatory oligodendrocyte. 445 Brain research 1641, 139-148, doi:10.1016/j.brainres.2015.09.021 (2016). 446 24 Peferoen, L., Kipp, M., van der Valk, P., van Noort, J. M. & Amor, S. 447 Oligodendrocyte-microglia cross-talk in the central nervous system. *Immunology* **141**, 302-448 313, doi:10.1111/imm.12163 (2014). 449 25 Zeis, T. & Schaeren-Wiemers, N. Lame ducks or fierce creatures? The role of 450 oligodendrocytes in multiple sclerosis. J Mol Neurosci 35, 91-100, doi:10.1007/s12031-008-451 9042-1 (2008). 452 26 Moyon, S. et al. Demyelination causes adult CNS progenitors to revert to an 453 immature state and express immune cues that support their migration. The Journal of 454 neuroscience : the official journal of the Society for Neuroscience 35, 4-20, 455 doi:10.1523/JNEUROSCI.0849-14.2015 (2015). 456 27 Huynh, J. L. et al. Epigenome-wide differences in pathology-free regions of multiple 457 sclerosis-affected brains. Nat Neurosci 17, 121-130, doi:10.1038/nn.3588 (2014). 458 Traka, M., Podojil, J. R., McCarthy, D. P., Miller, S. D. & Popko, B. 28 459 Oligodendrocyte death results in immune-mediated CNS demyelination. Nat Neurosci 19, 65-460 74, doi:10.1038/nn.4193 (2016). 461

462 Figure legends

- 463 Figure 1: Single cell RNA-sequencing of oligodendrocyte (OL) lineage cells in response
- 464 to experimental autoimmune encephalomyelitis (EAE) uncovers new disease-specific

465 populations and disease markers. a, Schematic overview of the methodology used to 466 perform single-cell RNA-seq of the OL lineage cells. b, Clinical score of the diseased animals 467 used in the study (n=12 mice; data represented as mean \pm s.e.m.; only animals that reached 468 score 3 and one that reached score 2.5 were used in this study). c, t-SNE plots of all cells 469 sequenced showing the segregation of cells derived from Complete Freund's Adjuvant (CFA) 470 controls and EAE (n=4 biologically independent mouse spinal cord samples per condition; 471 total number of cells is 794 for controls and 971 for EAE). d, t-SNE plots of all cells 472 sequenced representing different cell populations within OL lineage cells. Mature 473 oligodendrocyte (MOL) identities were defined according to marker genes identified in ref. 4 474 (n=4 biologically independent mouse spinal cord samples per condition; total number of cells 475 is 745 for controls and 707 for EAE). e-f, Violin plots depicting the expression of specific 476 markers for OL precursor cells (OPC) (e) and for MOL clusters (f) (n=4 biologically 477 independent mouse spinal cord samples per condition; total number of cells is 116 for OPC 478 controls and 132 for OPC EAE and 626 for MOL controls and 575 for MOL EAE). Violin 479 plots are centered around the median with interquartile ranges and shape represents cell 480 distribution. g, t-SNE plots of disease-specific markers for OL lineage cells (n=4 biologically 481 independent mouse spinal cord samples per condition; total number of cells is 745 for 482 controls and 707 for EAE). h, Schematic representation of the exon 6 inclusion in the Pdgfa 483 gene in response to EAE. i, Violin plot representing the PSI (proportion of spliced isoform) in 484 controls (MOL2 Ct-a depicted in green) and EAE (MOL1/2 EAE depicted in purple) of the 485 alternative spliced exons in *Pdgfa* and *Mbp* genes. PSI=0 means totally excluded and PSI=1 486 totally included (n=4 biologically independent mouse spinal cord samples per condition; total 487 number of cells is 56 for MOL2 Ct-a and 49 for MOL1/2 EAE; Pdgfa ex6: p=0.0003176 and 488 *Mbp* ex2: p=5.323e-11 by two-sided Wilcoxon rank sum test with continuity correction; 489 Violin plots are centered around the median with interquartile ranges and shape represents 490 cell distribution. VLMCs - vascular and leptomeningeal cells; MiGl - Microglia-like cells.

491

492 Figure 2: Expression of immunoprotective and adaptive immunity genes in response to 493 EAE. a, RNAscope ISH representing a spinal cord from CFA control and EAE mice marked 494 with probes for Sox10, Klk8 and Hopx, markers of MOL1/2-EAE. Dashed boxes shown at 495 higher magnification highlight regions with higher densities of MOL1/2 cells. Arrows depict 496 triple positive cells in EAE and arrowheads depict *Hopx* positive OL lineage cells negative 497 for Klk8. Representative images, n=3 biologically independent mouse spinal cord samples. 498 Scale bars - 20µm b, Violin plots representing Serpina3 family of genes in OL lineage cell 499 populations derived from CFA controls and EAE mice. (n=4 biologically independent mouse 500 spinal cord samples per condition; total number of cells is 745 for controls and 707 for EAE).

501 Violin plots are centered around the median with interquartile ranges and shape represents 502 cell distribution. c, RNAscope ISH representing a spinal cord from CFA control and EAE 503 mice marked with probes for Sox10 and Serpina3n. Representative images, n=3 biologically 504 independent mouse spinal cord samples. Scale bars - $20\mu m$. d, Violin plots representing MHC 505 class I related genes in OL lineage cell populations derived from CFA controls and EAE 506 mice. (n=4 biologically independent mouse spinal cord samples per condition; total number 507 of cells is 745 for controls and 707 for EAE). Violin plots are centered around the median 508 with interquartile ranges and shape represents cell distribution. e, RNAscope ISH 509 representing a spinal cord from CFA control and EAE mice marked with probes for Sox10, 510 and MHC-I related genes, *Psmb9* and *B2m*. Arrows depict triple positive cells, arrowheads 511 depict cells double positive for *Psmb9/B2m* and negative for *Sox10* that do not belong to the 512 OL lineage. Representative images, n=3 biologically independent mouse spinal cord samples, 513 scale bars - 20µm.

514

515 Figure 3: Expression of MHC class II and MS susceptibility genes in the OL lineage cells 516 in response to EAE and in MS. a Violin plots representing MHC class II related genes in 517 OL lineage cell populations derived from CFA controls and EAE mice. (n=4 biologically 518 independent mouse spinal cord samples per condition; total number of cells is 745 for 519 controls and 707 for EAE). Violin plots are centered around the median with interquartile 520 ranges and shape represents cell distribution. **b-d**, RNAscope ISH representing spinal cords 521 from CFA control and EAE mice marked with probes for MHC-II (Cd74), OL lineage cells 522 (Sox10 and Ptprz1/Pdgfra-H2B-GFP specific for OPCs) and microglia (Aif1). Dashed boxes 523 shown at higher magnification represent both OL lineage cells expressing MHC-II 524 (arrowhead), and microglia cells expressing MHC-II (arrow). Representative images, n=3 525 biologically independent mouse spinal cord samples per condition, scale bars - $20\mu m$. e, 526 Immunohistochemistry showing OL lineage cells (positive for Sox10) co-expressing MHC-II 527 protein, in a lesion in the spinal cord of EAE mice. Representative images, n=3 biologically 528 independent mouse spinal cord samples per condition, scale bars - $20\mu m$. f, 529 Immunohistochemistry in human samples from two MS patients representing OLIG1 positive 530 OLs expressing MHC-II (arrows). Representative images, n=2 biologically independent 531 human brain samples. Scale bars - 25µm. g, Expression-based heat maps for the MS 532 susceptibility genes (from ref. 1) in microglia and OL lineage cells. MHC locus and non-533 MHC locus related genes are represented in both microglia and all OL lineage cells 534 populations analyzed in this study.

Figure 4: OPCs express MHC-II in response to interferon- γ , exhibit phagocytic capacity and regulate T cell survival and proliferation. a, Schematic representation of co-culture

537 between OPCs isolated from Sox10-Cre-GFP mice and CD45+ immune cells isolated from 538 EAE mice or CFA controls. b, Immunohistochemistry showing OL lineage cells (positive for 539 Sox10) co-expressing MHC-II protein, but not the microglia marker IBA1, upon co-culture 540 with CD45+ immune cells from EAE mice. Representative images, n=3 independent 541 experiments, scale bars - $20\mu m$. c, Schematic representation of treatment of OPCs and OLs 542 with interferon- γ (100 ng/ml) and dexamethasone (1 μ M). d, OLs cultured with 543 dexamethasone and interferon- γ for 72h express MHC-II as represented by Cd74/Sox10 and 544 MHC-II/CNP double staining in RNAscope ISH and immunocytochemistry, respectively. 545 Representative images, n=3 independent experiments. Scale bars - 20µm. e, qRT-PCR 546 analysis for MHC and interferon responsive genes on primary OPCs and OLs treated with 547 interferon- γ and dexamethasone, n=3 independent experiments per condition; data 548 represented as mean \pm s.d. f, Uptake of pHrodo-labeled myelin and 1µm diameter fluorescent 549 microspheres by primary NG2+ OPCs after 6 and 24 hours, respectively, and upon treatment 550 with 50µM of cytochalasin D. Representative images, n=3 independent experiments. Scale 551 bars - $20\mu m$. g, Quantification of the percentage of OPCs uptaking microspheres in the 552 presence or absence of IFN- γ (100 ng/ml) and upon treatment with 20 and 50 μ M of 553 cytochalasin D. n=3 independent experiments per condition; data represented as mean \pm s.d. 554 **h**, Schematic representation of co-culture between primary OPCs, treated with interferon- γ 555 and/or MOG 35-55 peptide, and three different types of CD4 lymphocytes (naïve, memory 556 and activated Th1) from 2D2 transgenic mice, where a high proportion of CD4 T-557 lymphocytes express a T-cell receptor specific for MOG35-55 peptide. i-j, Graph plots 558 obtained from FACS analysis of naïve, memory and activated Th1 2D2 CD4 T cells after 72 559 hours of co-culture with OPCs. General survival (dead cell exclusion marker) and 560 proliferation (CD4⁺ V β 11⁺ Ki67⁺) were assessed. Numbers of cells in the live gate as well as 561 in the Ki67⁺ gate were estimated and reflect survival and proliferation since the same cell 562 numbers were seeded onto different wells. Plots represent the averages of the assessed values 563 for the different conditions divided by the values of the control (T cells only) for fold change 564 differences. n=7 independent experiments; data represented as mean \pm s.e.m.

565 **ONLINE METHODS**

566 Information regarding methods used in this paper can be found below and also in the Life 567 Sciences Reporting Summary.

568

Animals. Mouse lines used in this study included C57BL/6NJ wild type (WT) mice, Pdgfra-569 Cre-LoxP-GFP⁷, Pdgfra-H2B-GFP knock-in mice⁶, Sox10Cre-LoxP-GFP²⁹ and C57Bl/6 2D2 570 transgenic mice²². Pdgfra-Cre-LoxP-GFP mice are a strain of mice obtained originally by 571 572 crossing mice with Cre recombinase under the control of a Pdgfra genomic DNA fragment 573 (with a C57BL/6NJ genetic background; The Jackson Laboratories, CA, USA) with reporter 574 mice RCE:loxP-GFP (with CD1 background; Gord Fishell, NYU Neuroscience Institute) to label the complete OL lineage. Sox10-Cre-LoxP-GFP mice are a strain of mice obtained 575 576 originally by crossing mice with Cre recombinase under the control of the Sox10 promoter 577 (The Jackson Laboratories, CA, USA; with a C57BL/6 genetic background) with reporter 578 mice RCE:loxP-GFP (with CD1 background) to label the complete OL lineage. Pdgfra-579 H2B-GFP, with a C57BL/6NJ background, presents an H2B-eGFP fusion gene expressed 580 under the promoter of the OPC marker, *Pdgfra*. Mice homozygous for the knock-in targeted 581 mutation have an embryonic lethal phenotype, with half of the embryos failing to survive past 582 embryonic day 12.5 and the remainder failing to survive beyond embryonic day 15.5 583 (https://www.jax.org/strain/007669). Only heterozygote mice were used, in which Pdgfra is 584 expressed mainly in OPCs but also in some extent in the early stages of OL differentiation, 585 due to GFP half-life. Animals were used in adult stage, between 10-12 weeks old and both 586 genders were included. The following light/dark cycle was used: dawn 6.00-7.00; daylight 587 07.00-18.00; dusk 18-00-19.00; night 19.00-06.00. A maximum of 5 adult mice per IVC-cage 588 of type II Allentown. Breedings were done with 1 male and up to 2 females. All experimental 589 procedures performed followed the guidelines and recommendations of local animal 590 protection legislation and were approved by the local committee for ethical experiments on 591 laboratory animals in Sweden (Stockholms Norra Djurförsöksetiska nämnd).

592

593 **Experimental Autoimmune Encephalomyelitis (EAE).** For the induction of chronic EAE, 594 animals were injected subcutaneously with an emulsion of MOG35-55 in complete Freud's 595 adjuvant (CFA; EK-2110 kit from Hooke Laboratories) followed by the administration of 596 pertussis toxin in PBS ($0,2\mu g$ per animal), for two consecutive days (all according to 597 manufacturer's instructions). Spinal cords and cerebellum were collected at the peak/chronic 598 stage of the disease with clinical score=3 representing limp tail and complete paralysis of hind 599 legs. Animals that did not reach this clinical score were not analyzed in this study. Additional 600 animals were injected subcutaneously with a CFA emulsion (CK-2110 kit from Hooke 601 Laboratories) and analyzed as controls.

602

603 Tissue dissociation for single-cell RNA sequencing, FACS analysis and sequencing data 604 processing. Cells were isolated from the spinal cord of P90 Pdgfra-H2B-GFP and Pdgfra-605 Cre-LoxP-GFP mice. Tissue was then dissociated into a single cell suspension, as previously 606 described in Marques et al 2016, with some modifications. Mice were perfused with 607 oxygenated cutting solution (87 mM, NaCl, 2.5 mM KCl, 1.25 mM NaH2PO4, 26 mM 608 NaHCO3, 75 mM sucrose, 20 mM glucose, 1 mMCaCl2, and 2 mM MgSO4) and the brain 609 was quickly dissected and dissociated using the Adult brain dissociation kit from Miltenvi 610 (130-107-677) following the manufacturer's instructions (red blood cells removal step was 611 not included). After debris removal, cell suspension was filtered with 30µm filter (Partec) and 612 processed by FACS. Spinal cord single GFP⁺ cells were selected in a BD Influx sorter and collected into a 384 plate for SmartSeq2, according to procedures described in⁵. SmartSeq2 613 raw data was processed according to procedures described in⁵. Smart-seq2 paired-end reads 614 were trimmed with cutadapt 1.8.0³⁰ and aligned with STAR 2.5.1b³¹ to mm10 genome 615 616 assembly, only uniquely mapped reads were used for downstream analyses.

617

618 Primary OPC cell culture. Mice brains from P7 pups were removed and dissociated in 619 single-cell suspensions using the Neural Tissue Dissociation Kit (P; Miltenyi Biotec, 130-620 092-628) according to the manufacturer's protocol. OPCs were obtained with MACS with 621 CD140a microbeads following the manufacturer's protocol (CD140a Microbead kit, Miltenyi 622 Biotec 130-101-547). Alternatively to MACS, GFP+ OPCs derived from Sox10-GFP mice 623 were collected with FACS following brain dissociation. Cells were seeded in poly-L-lysine 624 (O/N; Sigma P4707) plus fibronectin (1h; Sigma F1141) coated dishes and grown on 625 proliferation media comprising DMEM/Gmax (ThermoFisher Scientific 10565018), N2 626 media (ThermoFisher Scientific 17502048), Pen/Strep (ThermoFisher Scientific 15140122), 627 NeuroBrew (Miltenyi 130-093-566), bFGF 20ng/ml (Peprotech 100-18B) and PDGF-AA 628 10ng/ml (Peprotech, 100-13A). For OPC differentiation, cells were left for 2 days in medium without bFGF and PDGF-AA. Cells were treated either with Dexamethasone (1µM), 629 630 Interferon-gamma (100ng/mL; R&D, 485-MI-100) or the combination of the two for 72 631 hours. For the phagocytosis experiments, 1µL per ml of media of pHrodo-labeled myelin and

0.5μL per ml of media of Fluoresbrite® Polychromatic Red Microspheres 1μm (Polysciences,
Inc, 18660-5) were added to OPCs for 6h and 24h, respectively. Hoechst (ThermoFisher
Scientific, 62249) was added at a dilution 1:1000 to OPCs incubated with pHrodo-labeled
myelin for live-cell fluorescent staining of the DNA and nuclei. Phagocytosis inhibition
experiments were performed by adding two different concentrations of cytochalasin D
(Sigma, C8273) 20μM and 50μM in the presence or absence of Interferon-gamma
(100ng/mL) for 24 hours. Cells were thoroughly washed before fixation.

639 pHrodo-labeled myelin preparation: myelin sheaths were obtained by dissection and 640 mechanical homogenization of PBS perfused mouse brains. Pure myelin was then isolated by 641 several steps of density separation by ultra-centrifugation in sucrose solutions^{32,33}. After 642 several cleaning steps we incubated the purified myelin with pHrodo red (Thermo Fisher, 643 P36600) for 30 minutes following the manual instructions, followed by extensive washing in 644 PBS/Hepes.

645

646

647 **OPC/CD45+ EAE co-culture experiments.**

648 CFA and EAE mice were perfused in PBS and the spinal cords were collected. Immune cells 649 (lymphocytes, monocytes and macrophages) were then isolated using the adult Brain 650 Dissociation Kit (Miltenyi Biotec, 130-107-677) according to the manufacturer's protocol and 651 collected with MACS with CD45+ microbeads (CD45 Microbead kit, Miltenyi Biotec 130-652 052-301) according to the manufacturer's protocol. CD45⁺ cells (150-200,000) were added on 653 top of cultured OPCs (300,000 cells) and incubated for 72hours.

654

655 **OPC/T cell co-culture experiments.**

Naïve and memory T cells were isolated from C57Bl/6 2D2 transgenic mice that express a 656 TCR specific for the MOG 35-55 peptide²². Splenocytes were isolated by tissue disruption 657 658 through a 100µm mesh and erythrocytes were lysed with ACK buffer (Invitrogen). 659 Splenocytes were depleted from all non-T cells using a naive CD4⁺ T cell Isolation Kit (130-660 104-453; Miltenyi), and the flow through was further sorted into CD44 low (naïve) and CD44 661 high (memory) cells using anti-CD44 beads from the same kit. Cells were frozen in FCS 662 containing 10% DMSO for subsequent experiments. Activated T cells were generated from 663 naïve cells stimulated in vitro with plate-bound anti-CD3 (BD; 555273; 2µg/ml) and soluble 664 anti-CD28 (BD; 553294; 1µg/ml) in the presence of 10ng/ml IL-12 (R&D Systems, 419-ML) 665 for 3 days, followed by 3 days expansion in 10ng/ml IL-2 (R&D Systems, 402-ML) and 666 cytokine starvation for 24h prior to co-culture (at the exception of one n which was not 667 deprived from cytokines).

OPCs (6 n's obtained with MACS and one n with FACS of GFP+ cells from Sox10-GFP 668 669 mice) were seeded at a density of 20,000 cells per well in a 96-well plate and pre-treated with 670 interferon-gamma (100ng/mL) and/or MOG 35-55 peptide (Anaspec, AS-60130-5) at 671 40µg/ml for 72hours. Cells were washed twice in PBS. Naïve, memory and activated T cells 672 were both seeded alone (with or without MOG 35-55 peptide at $40\mu g/ml$) and on top of control or stimulated OPCs at $2x10^5$ cells/well in 96 well plates with MOG 35-55 peptide at 673 674 40µg/ml and incubated at 37°C. Media used for T cells as well as for T cell:OPC co-culture 675 was RPMI (Sigma, R8758), 10% FBS (v/v; Sigma F7524), Penicillin-Streptomycin (Sigma, 676 P4458, 100 U/ml). After 72h, cells were stimulated for 5h at 37°C in media containing 677 50ng/ml PMA (Sigma, P1585), 1µg/ml Ionomycin (Sigma, I0634) and 1µg/ml GolgiPlug 678 (BD, 555029), to boost cytokine secretion, followed by staining for CD4 PE-Dazzle (BioLegend, 100566), Ki67 V450 (BD, 561281), anti-TCR Vbeta11 BV510 (BD, 743677), 679 680 TNF PE-Cy7 (eBioscience, 25-7423-82), IFNg APC (BD, 554413) as well as dead cell 681 exclusion dye near-IR (Invitrogen, L10119). Surface staining at 4°C for 30 minutes was 682 followed by fixation and permeabilization using an intracellular staining kit (eBioscience, 88-683 8824-00), followed by intracellular staining. For the relative assessment of cell survival and 684 proliferation, samples were resuspended in equal volume and acquired by fixed time with a 685 Gallios Flow Cytometer (Beckman Coulter) and analyzed using a Kaluza Flow Cytometry 686 Analysis Software (Beckman Coulter). Numbers of cells in the live gate as well as in the 687 Ki67-positive gate reflect survival and proliferation since the same cell numbers were seeded 688 onto different wells. All conditions were run in three biological replicates for each of the 689 seven experiments. Averages of the assessed values for the different conditions were divided 690 by the values of the control (T cells only) for fold differences.

691

RNA extraction, cDNA synthesis and quantitative real-time PCR (qRT-PCR). Spinal 692 693 cord and cerebellum were collected from WT control and EAE mice. OPCs and OLs from in 694 vitro cultures were collected in 700µl Qiazol. RNA was extracted with the miRNeasy 695 microkit (Oiagen, 217084) according to manufacturer's protocols. Contaminating DNA was 696 degraded by treatment of the samples with RNase-free DNase (Qiagen, 79254) in column. 697 0.35-1µg of RNA from each sample was reversed transcribed for 1h with the High-Capacity 698 cDNA Reverse Transcription Kit (Applied Biosystems, 4368813) including RNase inhibitor 699 (Applied Biosystems, N8080119). A reverse transcriptase negative (RT-) control was

included for each sample. Both the cDNA and the RT- were diluted 1:5 in RNase/DNAse free

701 water for qRT-PCR.

702 qRT-PCR reactions were run on a StepOnePlus[™] System (Applied Biosystems) in duplicate 703 and with RT- reactions to control for genomic DNA. Fast SYBR® Green Master Mix 704 (Applied Biosystems, 4385616) was used according to the manufacturer's instructions, each 705 PCR reaction had a final volume of 10ul and 1–2.5ul of diluted cDNA or RT-. The running 706 conditions were 20 seconds at 95°C, followed by 40 cycles of 3 seconds of 95°C and 30 707 seconds of 60°C, then 15 seconds at 95°C, 1 minute at 60°C and 15 seconds at 95°C. A 708 melting curve was obtained for each PCR product after each run, to control for primer dimers 709 and gene-specific peaks. Tbp and Gapdh were run as housekeeping genes. Relative standard 710 curves were generated for each gene to determine relative expression (CT values are converted to arbitrary quantities of initial template per sample). Expression levels were then 711 712 obtained by dividing the quantity by the value of the geometric mean of the housekeeping genes. PCR primers sequences (design according ³⁴) used are the following: *Pdgfa short* (F: 713 714 CGTCAAGTGCCAGCCTTC and R: GCACACTCCAGGTGTTCCTC), Pdgfa long (F: 715 TGAAAGAGGTCCAGGTGAGG and R: CCTTTTCCTTTTCCGCTTTT), Mbp exon2 (F: 716 GCTTCTTTAGCGGTGACAGG and R: CCTTGTACATGTGGCACAGC), Mbp exon1 (F: 717 TGGCCACAGCAAGTACCAT and R: AGTCAAGGATGCCCGTGT), Tbp (F: 718 GGGGAGCTGTGATGTGAAGT and R: CCAGGAAATAATTCTGGCTCA), Gapdh (F: 719 GAGAAACCTGCCAAGTA and R: AGACAACCTGGTCCTCA), *Cd74* (F: 720 CTGGATGAAGCAGTGGCTCT and R: CCCAGGCCAGAAGATAGGTC), Ciita (F: 721 CTGGCACAGGTCTCTCCAGT and R: TACTGAGGCTGCTTGAAGGG), Nlrc5 (F: 722 CCGTGGTACTCACATTTGCC and R: CCTTCGAGATCTCTGGGACA), Ifit2 (F: 723 AAGGCAGAGGAAGAGGTTGC and GTCGCAGATTGCTCTCCAGT), Ifih1 (F: 724 ATGTCTTGGACACTTGCTTCG and R: CTGACTCATTCCCGCTGTTT) and Plin4 (F: 725 ACACAGTGGCCACAGGACTT and R: GGTCACCGTGTCCTTAGTGC).

726

727 Tissue processing for Immunofluorescence and **RNAscope** ISH. For 728 immunohistochemistry and RNAscope ISH mice were perfused with PBS followed by 4% 729 PFA. Spinal cords from EAE and control mice were dissected and post-fixed with 4% PFA 730 for 1h, at 4°C. The tissues were embedded into OCT (Tissue-Tek), frozen in dry ice and 731 sectioned coronally (20 μ m thickness). Sections were stored at -80° C.

For immunocytochemistry and RNAscope ISH in cultured cells, cells were fixed in 4%formaldehyde for 10 minutes and washed in PBS.

734

735 Immunohistochemistry and immunocytochemistry (mouse and human samples). For 736 immunocytochemistry cells were incubated overnight at 4°C with the following primary 737 antibodies: CNP (Abcam ab6319, Mouse 1:200), MHC-II (anti-I-A/I-E; BD Bioscience rat 738 1:600), GFP (Abcam ab13970, Chicken 1:1000), NG2 (Millipore AB5320, Rabbit 1:200), 739 IBA-1 (Wako 019-19741, rabbit 1:400) in PBS/0.5%Triton/10% normal donkey serum 740 (Sigma, D9663). Cells were washed with PBS and then incubated for 2 hours with Alexa 741 Fluor-conjugated antibodies (Invitrogen). 742 Spinal cord sections were incubated overnight at 4°C in the following primary antibodies:

743 OLIG2 (R&D, Goat 1:200), SOX10 (R&D, Goat 1:100), PLIN4 (Sigma, Rabbit 1:200), IBA-744 1 (Wako 019-19741, rabbit 1:400) and MHC-II (anti-I-A/I-E; BD Bioscience rat 1:600) 745 diluted in PBS/0.5% Triton/10% normal donkey serum. After washing the section with PBS, 746 secondary Alexa Fluor-conjugated antibodies (Invitrogen) diluted in PBS/0.5% Triton/10% 747 normal donkey serum were incubated for 2h at room temperature. Slides were mounted with 748 mounting medium containing DAPI (Vector, H-1200) and kept at 4°C until further 749 microscopic analysis. Images from sections were taken of the spinal cord using a Zeiss 750 LSM700 Confocal, and processed in ImageJ.

751 Human brain 4µm paraffin sections, from regions with high microglia activity (thus active 752 lesions) were dewaxed in a descending EtOH-row. After antigen retrieval and endogenous 753 peroxidase quenching, they were incubated over night at 4 degrees with the following primary 754 antibodies: OLIG1 (Abcam, 68105, 1:100), OLIG2 (Atlas, HPA003254, 1:200) and MHC-II 755 (Dako, M0775 1:100) diluted in TBS/0.3% Triton/20% normal horse serum. After washing 756 with TBS/0.001% Triton, they were incubated for 1 hour at room temperature with Goat F(ab) 757 Anti-Rabbit IgG H&L (HRP) and Goat F(ab) Anti-Mouse IgG H&L (HRP; ab7171 and 758 ab6823 abcam, 1:500). After washing in TBS/0.001% Triton, the fluorescence was visualized 759 with the tyramide kits from Perkin Elmer (NEL745B001KT and NEL744B001KT). The 760 human tissue used in this study comprised one female and one male, with ages of 38 and 50 761 years old both with secondary progressive multiple Sclerosis. No patient had specific disease 762 treatment. Post mortem MS tissue was provided via a UK prospective donor scheme with full 763 ethical approval from the UK Multiple Sclerosis Tissue Bank (MREC/02/02/39).

764

RNAscope ISH. RNAscope ISH was performed on cultured cells and spinal cord sections
from controls and EAE mice with probes for mouse *Cd74*, *H2-Eb1*, *Aif1*, *Sox10*, *Klk6*, *Hopx*, *Ptpzr1*, *Serpina3n*, *B2m*, *Psmb9* and *Klk8* all purchased from ACD. RNAscope ISH protocol

768 for sections was performed following manufacturer's instructions with minor modifications 769 (ACD, RNAscope® Multiplex Fluorescent Detection Reagents v2 Cat. No.323110). Briefly, 770 sections were placed on a hot plate (100°C) with 1x target retrieval (Pretreatment Reagents 771 Cat. No. 322381 and 322000) for 5 min followed by 2 steps of washes of 2 min and 1 wash 772 with 100% ethanol for 2min. Protease IV was applied on top of the sections and incubated for 773 20min at RT followed by 2 washes of 2 min each. Probes were diluted 1:50 in the C1 probe, 774 hybridized for 2h at 40°C and washed twice in wash buffer (RNAscope® Wash Buffer 775 Reagents Cat. No. 310091). Amplification steps were performed by incubating with v2Amp1 776 (30min), v2Amp2 (30min) and v2Amp3 (15min) at 40°C with washes of 2x2min in between 777 steps (RNAscope® Multiplex Fluorescent Detection Reagents v2 Cat. No. 323110). Sections 778 were incubated v2HRP-C1 for 15min at 40°C and washed twice in wash buffer for 2min. 779 TSA conjugated fluorophores were diluted in 1:1500 in TSA buffer (RNAscope® Multiplex 780 TSA Buffer Cat. No. 322809) and incubated for 30min at 40°C followed by 2 washes of 2min 781 and HRP blocker incubation for 30min at 40°C. The last steps were performed subsequently 782 for v2HRP-C2 and v2-HRP-C3. To combine the RNAscope ISH with immunofluorescence 783 for GFP, sections were further blocked in block with 5% NDS in 0.3% PBS-Tx100, 1h, RT 784 and incubated with chicken anti-GFP (abcam, ab13970 1:200,) overnight at 4°C. Sections 785 were further incubated with goat anti-chicken (Alexa Fluor 488 1:500) for 2h at RT and with 786 DAPI (1:5000) for 2 min.

787

788 Confocal Microscopy and cell counting. Images from sections of both Immunofluorescence 789 and RNAscope ISH were acquired for the spinal cord using a Zeiss LSM700 Confocal, and 790 processed in Fiji/ImageJ. Images from the human tissue were acquired using a Leica SP8 791 Confocal, Images were processed in Fiji/ImageJ. Estimation of the percentage of the double 792 MHC-II/SOX10 positive cells in the spinal cord of EAE mice was performed by counting the 793 double positive cells present in the lesion areas of the white matter divided by the total 794 SOX10+ cells. The final percentage is represented as an average of 3 EAE mice. For the co-795 cultures the number of GFP/MHC-II double positive cells were divided by the total number of 796 GFP+ cells. The final percentage is represented as an average of 3 independent experiments. 797 For estimation of the percentage of OPCs that phagocyte microspheres, only OPCs with more 798 than 10 microspheres surrounding the nucleus were considered as phagocytic OPCs. While 799 this might have led to an underestimation of phagocytic OPCs, this way we have avoided 800 counting OPCs with adherent and extracellular microspheres as phagocytic OPCs. Videos 801 were obtained from z-stacks after processing with Imaris image analysis software.

802

803 Supplementary Video information

Movie 1: **MOL2 cells express MHC-II genes.** RNAscope ISH representing a mouse spinal cord from EAE mice marked with probes for *Cd74* (red dots) and *Klk6* (green dots). A double positive cell is further highlighted in the video and represents an MOL2 cell expressing MHC-II.

- 808 Movie 2: OPCs express MHC-II genes. RNAscope ISH representing a mouse spinal cord
- 809 from EAE mice marked with probes for Cd74 (red dots), nuclear GFP (from Pdgfra-H2B-
- 810 GFP knock-in mice labeling OPCs) and *Ptprz1* (white dots). A triple positive cell is further
- 811 highlighted in the video and represents an OPC expressing MHC-II.
- 812 Movie 3: OL lineage cells express MHC-II genes. RNAscope ISH representing a mouse
- spinal cord from EAE mice marked with probes for Cd74 (red dots), Sox10 (green dots) and
- 814 Aif1 (white dots). A double positive cell is further highlighted in the video and represents an
- 815 OL lineage cell expressing MHC-II.
- 816 Movie 4: OL lineage cells express MHC-II genes. RNAscope ISH representing a mouse
- spinal cord from EAE mice marked with probes for Cd74 (red dots), Sox10 (green dots) and
- 818 Aif1 (white dots). A double positive cell is further highlighted in the video and represents an
- 819 OL lineage cell expressing MHC-II.
- 820 Movie 5: **OL lineage cells express MHC-II genes and few Aif1 molecules.** RNAscope ISH 821 representing a mouse spinal cord from EAE mice marked with probes for *Cd74* (red dots),
- 822 Sox10 (green dots) and Aif1 (white dots). At least 2 double positive cells are further
- highlighted in the video and represent an OL lineage cells expressing MHC-II and few *Aif1* molecules.
- 825 Movie 6: OL lineage cells express MHC-II genes. RNAscope ISH representing a mouse
- spinal cord from EAE mice marked with probes for *H2.eb1* (red dots) and *Sox10* (green dots).
- A double positive cell is further highlighted in the video and represents an OL lineage cell
- 828 expressing MHC-II.
- 829 Movie 7: **Microglia processes touch OL lineage cells.** RNAscope ISH representing a mouse 830 spinal cord from EAE mice marked with probes for *Cd74* (red dots), *Sox10* (green dots) and
- 831 Aifl (white dots). A microglia-derived process touching an OL lineage cell is further
- 832 highlighted in the video.
- 833 Movie 8: MHC-II positive cells surround OL lineage cells in human MS patient samples.
- 834 IHC performed in human brain tissue from one MS patient marked with antibodies for MHC-
- 835 II (white) and OLIG1 (green). A MHC-II positive cell that resides between two OLIG1

836 positive cells is further highlighted.

Movie 9: OL lineage cells from human MS patient samples express MHC-II genes. IHC
performed in human brain tissue from one MS patient marked with antibodies for MHC-II (white) and
OLIG1 (green). A double positive cell representing an OL lineage cell expressing MHC-II is further
highlighted in the video.

- 841
- 842

843 Clustering analysis using GeneFocus pipeline.

844 Quality Control. Cells were clustered using a custom-made approach, which we developed 845 and refer as GeneFocus. We generated an iterative Level 1 and Level 2 clustering pipeline, 846 taking advantage of diffusion mapping and spatial autocorrelation metrics to define relevant 847 genes and cell clusters. First cells were analysed and quality control (OC) filtering was 848 applied using the scater 1.6.0 in R. We applied cut-offs for the expression level 200000 total 849 FPKM and number of genes expressed 2500, resulting in 2304 and 1777 cells pre- and -post 850 QC respectively. Median FPKM values were 395721, and median gene counts were 3694 851 genes.

852

853 **Spatial Gene-filtering.** Cells were normalized (see supplemental code in Github) and feature 854 selection was performed using a support vector model from the e1071 R package 855 (https://CRAN.R-project.org/package=e1071). The resulting expression matrix was then inputted into 856 a custom pipeline performing iterative gene-filtering in the following manner: we converted the expression matrix into a transition matrix using destiny 2.6.1 in R^{35} with the input being 857 858 the first 30 principal components of the expression matrix. Subsequently, a distance matrix 859 was created from the transition matrix, after which the MoransI autocorrelation metric was computed for each gene using the spdep 0.6-15 R package³⁶. Genes were filtered according to 860 861 the mean MoransI computed for all the genes in the expression matrix, and this mean MoransI 862 was set as a general threshold for subsequent gene filtering. After this initial filtering, a new 863 diffusion map was computed and we iteratively repeated this process until all genes within the 864 gene set remained above the determined threshold of spatial correlation set during the first 865 round of gene filtering. A similar approach was performed using the transition matrix as a 866 distance metric. A cut-off value was calculated using a support vector model that predicts a 867 mean distance as a function of the population size in which the gene is expressed and the 868 mean distance observed. We iterated the distance matrix until we obtained a gene set equal or 869 smaller than the covered gene set obtained from the MoransI metric. A joint diffusion map

was then created.

871

Level 1 Clustering. Level 1 clustering was established by estimating the ideal number of clusters by silhouette width using the principal components of the transition matrix, from which the number was estimated on the basis of an elbow plot. We estimated clusters using the factoextra 1.0.5 package (https://CRAN.R-project.org/package=factoextra) and hierarchical clustering using Wards metric. We determined 5 initial clusters representing OPCs and early OLs, MOLs, VLMCs and pericytes, and microglial cells.

878

879 Level 2 Clustering. To determine more specific clustering and relevant genes we performed 880 the iterative gene filtering on each of the subclusters. The threshold for the MoransI metric 881 was established to be the mean MoransI of the gene set resulting from the second gene 882 filtering round. This resulted in a final gene set for each sub-cluster varying between 800-883 1000 spatially correlated genes per Level 1 sub-cluster. Clusters were estimated by silhouette 884 width and the final clustering was evaluated using the resulting heatmap of the filtered genes. 885 For validation of the GeneFocus pipeline, we extracted the expression information from GEO from³⁷ and were able to identify the disease-associated microglia cluster previously 886 described³⁷ (Supplementary Fig. 2). To achieve out final clustering result, we also removed 887 888 cells that were clustered in clusters with less than 3 cells, resulting in a total number of 1765

cells. These cells seemed to be doublets based on mixed expression profiles.

889 890

891 Gene Modules. To generate the gene-modules, we performed non-negative matrix 892 factorization, where ranks were established using a measure of mutual information with the 893 elbow method. We established that 30 ranks were the optimal rank to decompose the dataset 894 in. To only select robust components from the decomposed matrix, we performed PCA on the 895 components and established an optimal k number of clusters based on wards metric. All 896 component values falling within a cluster were summed after which the new concatenated 897 components were filtered based on a threshold of a Pearson correlation of 0.5 with any gene 898 in the dataset. This resulted in 15 components that revealed the major gene trends underlying 899 the data.

900

901 Differential expression and pathway visualization

902 Differential expression analysis was performed using the MAST R package v1.4.1³⁸. Pathway 903 visualization was performed using the clusterProfiler package v3.6.0³⁹. 904

Comparison between OPCs in the current dataset and OPCs during development⁴. The
R package MetaNeighbor was used, found at (https://github.com/maggiecrow/MetaNeighbor).

- 907
- 908

909 Gene ontology and pathway analysis. Most significantly differentially expressed genes were 910 selected for each of the GO analyses. For each cell type, unique top differentially upregulated 911 genes in EAE and unique top differentially upregulated genes in controls were selected. For 912 comparisons between cell types, uniquely differentially expressed genes for each cell category 913 were selected. In order to make gene sets comparable, top 100 genes were selected. GO and pathway analysis was performed with Cytoscape 3.5.1⁴⁰ plug-in ClueGO v2.3.3⁴¹ with 914 915 settings, GO Biological process (23.02.2017) and REACTOME pathways (01.03.2017), 916 showing only pathways with P-val ≤ 0.05 , minimum 5 genes per cluster, and default 917 settings.

918 In accordance with the NNMF analysis, OPCs and OLs from EAE mice shared an enrichment 919 for genes involved in the positive regulation of adaptive immune response, positive regulation of T cell mediated cytotoxicity, response to interferon and antigen processing and 920 921 presentation of endogenous peptides via MHC-I (Supplementary Fig. 4b). GO/Reactome 922 analysis for the enriched genes in individual clusters indicated that OPC2-EAE was enriched 923 in positive regulation of T cell mediated cytotoxicity, antigen presentation, among other 924 processes (Supplementary Fig. 5). MOL1/2-EAE exhibited enrichment in similar processes, 925 but also additional processes related with glycosylation (Supplementary Fig. 5), which has been implicated in the activation of adaptive immune activation⁴². In contrast to these 926 927 populations, "young" (Pdgfra-H2B-GFP) MOL5/6-EAE-a exhibited less pronounced 928 upregulation in immune related GO-terms (Supplementary Fig. 5). Instead, this Plin4⁺ MOL 929 cluster is enriched in genes related to lipid modification, gliogenesis, and intrinsic apoptotic 930 signaling pathway (with anti-apoptotic genes Bcl211, Cdkn1a and pro-apoptotic genes Bnip3, 931 *Ppp1r13b*; Supplementary Table 1), among other categories (Supplementary Fig. 5).

- 932
- 933

Alternative splicing analysis. Alternatively spliced cassette exons were identified with BRIE
 0.1.3⁴³ in the cell types clusters from Smart-seq2 data. Cassette exons annotations were
 extracted from Gencode.vM12 from protein-coding genes according to the parameters in ⁴³.
 For each of the cells classified as MOL1/2, MOL5/6 and OPC, the fraction of exon inclusion

938 was calculated (PSI), with default parameters. Then, for each cell type, cell to cell pair-wise 939 comparisons were performed, comparing EAE-assigned with control-assigned cells. 940 Significantly alternative spliced candidates were selected with the following parameters, 941 Bayes factor > 10, delta PSI between the two cells > 0.2 and a minimum number of 942 significant comparisons for each cell type (MOL12 ≥ 20 , OPC ≥ 20 and MOL56 ≥ 100). 943 In order to get more specific alternatively spliced exons, the candidate events were selected 944 only when they were uniquely spliced in one direction for each cell type, for instance events 945 that are only skipped in EAE and events only included in EAE. Violin plots of selected events 946 were plotted using all the PSI values for that specific alternative exon in EAE and in control, 947 Wilcoxon rank sum test with continuity correction was used for significance test. 948 Visualization of the alternative spliced events junctions reads was done with the merged bam files and the sashimi plot option in IGV⁴⁴. 949

950

MS susceptibility genes. Genes assigned to human MS susceptibility SNPs were transform to
 Mus musculus annotation using BioMart ⁴⁵. Human chrX associated SNPs from ref 2 were
 assigned to hg19 GENCODEv19 gene annotations with Bedtools v2.25.0⁴⁶, with parameters
 windowbed -60000. Recovered genes were transform to *Mus musculus* gene symbols using
 BioMart.

956

957 Ethics approval and consent to participate. The collection of all animal samples was 958 performed according to the guidelines and recommendations of local animal protection 959 legislation and were approved by the local committee for ethical experiments on laboratory 960 animals in Sweden (Stockholms Norra Djurförsöksetiska nämnd). Human post mortem MS 961 tissue was provided via a UK prospective donor scheme with full ethical approval from the 962 UK Multiple Sclerosis Tissue Bank (MREC/02/02/39). All participants gave prospective pre-963 mortem written consent for their brains to be banked and used for research.

964

Code availability. Code used for single cell RNA-Seq analysis is available at
 <u>https://github.com/Castelo-Branco-lab/GeneFocus</u>.

967

968 Data availability: A web resource for browsing differential gene expression data for the 969 single cell data can be accessed at <u>https://ki.se/en/mbb/oligointernode</u>. Raw data is deposited 970 in GEO, accession number GSE113973. Code used for single cell RNA-Seq analysis is 971 available at <u>https://github.com/Castelo-Branco-lab/GeneFocus</u>. 972

973 Supplementary Table information

974 Supplementary Table S1 – Differential gene expression and gene module associated with clusters

975 (level 1 and level 2 - oligodendrocytes) identified by single cell RNA-Seq in CFA and EAE mice. n=4
976 biologically independent mouse spinal cord samples per condition.

977 Supplementary Table S2 - Splicing events and exon inclusion or exclusion events summarized by

cluster, in single cell RNA-Seq in CFA and EAE mice. n=4 biologically independent mouse spinalcord samples per condition.

980

981 Supplementary Table S3 - Differential genes expression between CTRL and EAE in MOLs and 982 OPCs and Gene Ontology terms for comparisons, enriched genes for each cluster, and alternatively 983 spliced genes between CTRL and EAE. n=4 biologically independent mouse spinal cord samples per 984 condition. All GO analysis where performed in cytoscape and p <0.05; p values were calculated with 985 Bonferroni two-sided hipergeometric test.

986

987 Supplementary Table S4 - Non-MHC MS susceptibility genes expressed in microglia and OPCs in
 988 EAE and CTRL and significant differential expression across the major level 1 clusters.

- 989
- 990
- 991

992 29 Matsuoka, T. et al. Neural crest origins of the neck and shoulder. Nature 436, 347-355, 993 doi:10.1038/nature03837 (2005). 994 Martin, M. Cutadapt removes adapter sequences from high-throughput sequencing reads. 30 995 *EMBnet.journal* **17**, pp.-10-12, doi:10.14806/ej.17.1.200 (2011). 996 Dobin, A. et al. STAR: ultrafast universal RNA-seq aligner. Bioinformatics 29, 15-21, 31 997 doi:10.1093/bioinformatics/bts635 (2013). 998 32 Norton, W. T. & Poduslo, S. E. Myelination in rat brain: method of myelin isolation. J 999 Neurochem 21, 749-757 (1973). 1000 Larocca, J. N. & Norton, W. T. Isolation of myelin. Curr Protoc Cell Biol Chapter 3, Unit3 33 1001 25, doi:10.1002/0471143030.cb0325s33 (2007). 1002 Zeisel, A., Yitzhaky, A., Bossel Ben-Moshe, N. & Domany, E. An accessible database for 34 1003 mouse and human whole transcriptome qPCR primers. *Bioinformatics* **29**, 1355-1356, 1004 doi:10.1093/bioinformatics/btt145 (2013). 1005 Angerer, P. et al. destiny: diffusion maps for large-scale single-cell data in R. Bioinformatics 35 1006 32, 1241-1243, doi:10.1093/bioinformatics/btv715 (2016). 1007 36 Bivand, R., Hauke, J. & Kossowski, T. Computing the Jacobian in Gaussian Spatial 1008 Autoregressive Models: An Illustrated Comparison of Available Methods. Geographical Analysis 45, 1009 150-179, doi:doi:10.1111/gean.12008 (2013). 1010 37 Keren-Shaul, H. et al. A Unique Microglia Type Associated with Restricting Development of

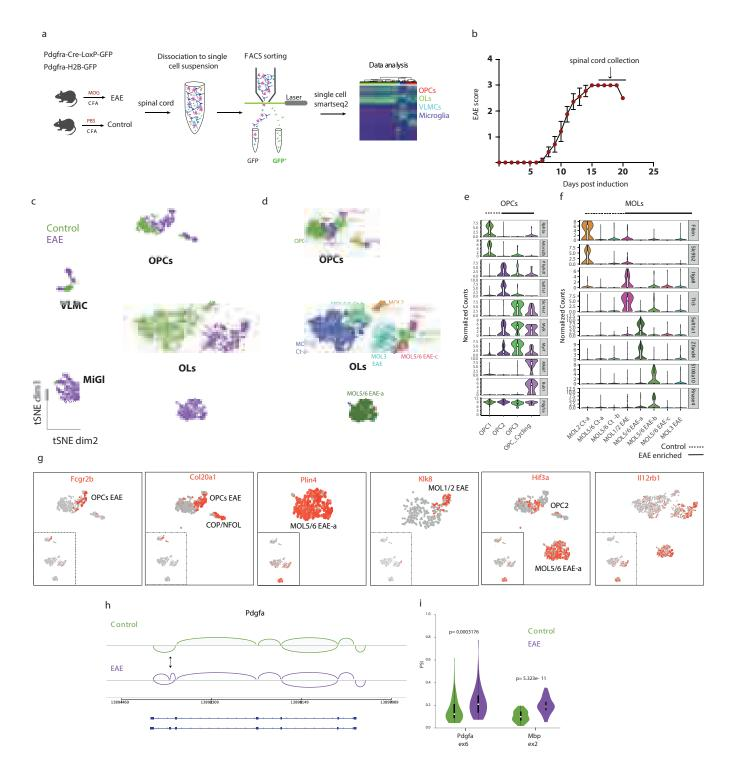
1011 Alzheimer's Disease. *Cell* **169**, 1276-1290 e1217, doi:10.1016/j.cell.2017.05.018 (2017).

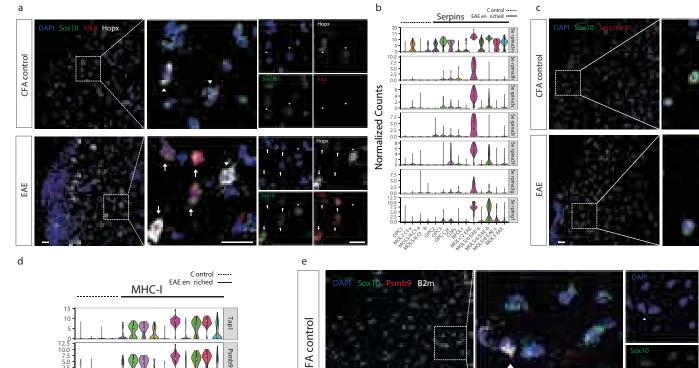
1012 38 Finak, G. *et al.* MAST: a flexible statistical framework for assessing transcriptional changes
1013 and characterizing heterogeneity in single-cell RNA sequencing data. *Genome biology* 16, 278,
1014 doi:10.1186/s13059-015-0844-5 (2015).

29

- 1015 39 Yu, G., Wang, L. G., Han, Y. & He, Q. Y. clusterProfiler: an R package for comparing
- 1016 biological themes among gene clusters. OMICS 16, 284-287, doi:10.1089/omi.2011.0118 (2012).
- Killcoyne, S., Carter, G. W., Smith, J. & Boyle, J. in *Protein Networks and Pathway Analysis Methods in Molecular Biology* 219-239 (Humana Press, 2009).
- 1019 41 Bindea, G. *et al.* ClueGO: a Cytoscape plug-in to decipher functionally grouped gene ontology 1020 and pathway annotation networks. *Bioinformatics* **25**, 1091-1093, doi:10.1093/bioinformatics/btp101 1021 (2009).
- 1022 42 Wolfert, M. A. & Boons, G. J. Adaptive immune activation: glycosylation does matter. *Nature* 1023 *chemical biology* **9**, 776-784, doi:10.1038/nchembio.1403 (2013).
- Huang, Y. & Sanguinetti, G. BRIE: transcriptome-wide splicing quantification in single cells.
 Genome Biol 18, doi:10.1186/s13059-017-1248-5 (2017).
- 1026 44 Thorvaldsdóttir, H., Robinson, J. T. & Mesirov, J. P. Integrative Genomics Viewer (IGV):
- high-performance genomics data visualization and exploration. *Brief Bioinform* 14, 178-192,
 doi:10.1093/bib/bbs017 (2013).
- 1029 45 Durinck, S., Spellman, P. T., Birney, E. & Huber, W. Mapping identifiers for the integration 1030 of genomic datasets with the R/Bioconductor package biomaRt. *Nat. Protoc.* **4**, 1184-1191 (2009).
- 1031 46 Quinlan, A. R. BEDTools: the Swiss-army tool for genome feature analysis. *Current*
- 1032 protocols in bioinformatics / editoral board, Andreas D. Baxevanis ... [et al.] 47, 11.12.11-11.12.34,
- 1033 doi:10.1002/0471250953.bi1112s47 (2014).

1034 1035







а

Normalized Counts

0 12.5 10.0 7.5 5.0 2.5 0.0 15 10 0-15-10 ,1 15 -10 -5 <u>71</u> 10 -5 -0 -100,00C

6

B2m

H2.K1

H2.D1

H2.T23

b

Control ······ EAE en riched -----

